Journal of Power Sources 227 (2013) 254–259

Contents lists available at SciVerse ScienceDirect

Journal of Power Sources

journal homepage: www.elsevier.com/locate/jpowsour

MnO_2-coated graphitic petals for supercapacitor electrodes

Guoping Xiong [a,b], K.P.S.S. Hembram [a,b], R.G. Reifenberger [a,c], Timothy S. Fisher [a,b,*]

[a] Birck Nanotechnology Center, Purdue University, West Lafayette, IN 47907, USA
[b] School of Mechanical Engineering, Purdue University, West Lafayette, IN 47907, USA
[c] Department of Physics, Purdue University, West Lafayette, IN 47907, USA

HIGHLIGHTS

- Buckypaper modified by graphitic petals to enhance area and chemical functionality.
- MnO_2 coated on the carbon structure by a simple, solution-based method.
- Exceptional functional performance: 580 F g^{-1} (MnO2 mass basis), 44 Wh kg^{-1}, 25 kW kg^{-1}.
- Less than 10% degradation after 1000 CV cycles.

GRAPHICAL ABSTRACT

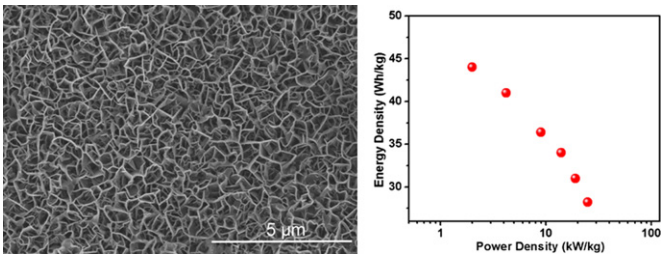

ARTICLE INFO

Article history:
Received 24 July 2012
Received in revised form
24 October 2012
Accepted 14 November 2012
Available online 28 November 2012

Keywords:
Manganese dioxide
Graphitic petals
Supercapacitor
Carbon nanotubes
Electrodes

ABSTRACT

Hybrid manganese dioxide/graphitic petal structures grown on carbon nanotube substrates are shown to achieve high specific capacitance, energy density, power density, and long cycle life for flexible supercapacitor applications. Vertical nanoscale graphitic petals were prepared by microwave plasma chemical vapor deposition on commercial carbon nanotube substrates and subsequently coated with a thin layer of MnO_2. The graphitic petal/carbon nanotube architecture without any binder provides an efficient scaffold for maximizing the electrochemical performance of MnO_2. A specific capacitance (based on the mass of MnO_2) of 580 F g^{-1} is obtained at a scan rate of 2 mV s^{-1} in 1 M Na_2SO_4 aqueous electrolyte. The energy density and power density at 50 A g^{-1} are 28 Wh kg^{-1} and 25 kW kg^{-1}, respectively. In addition, the composite electrode shows excellent long-term cyclic stability (less than 10% decrease in specific capacitance after 1000 cycles) while maintaining a small internal resistance. Parallel density functional studies were performed to investigate the stability and electronic structure of the MnO_2/graphene interface. Taken together, the work indicates the MnO_2/graphitic petal/carbon nanotube composite is a promising electrode material for high-performance supercapacitors.

1. Introduction

Electrochemical capacitors (ECs), known as supercapacitors or ultracapacitors, with high power density, fast power delivery and long cycle life, promise to complement or even replace batteries in energy storage applications such as uninterruptible back-up power supplies, load-leveling, portable electronics, hybrid electronic vehicles and renewable energy systems [1,2]. To achieve high power and high energy density, suitable electrode materials are required to undergo fast reversible redox reactions. Metal oxides (*e.g.*, MnO_2 [3], RuO_2 [4], VO [5], Fe_2O_3 [6]) offer high pseudocapacitance through fast and reversible redox reactions near the surface of active materials. Because of its high specific capacitance (720 F g^{-1}) [4], RuO_2 is one of the most promising candidates for ECs. However, commercialization of RuO_2 is unlikely because of its

* Corresponding author. School of Mechanical Engineering, Purdue University, West Lafayette, IN 47907, USA. Tel.: +1 765 494 5627; fax: +1 765 494 0539.
E-mail address: tsfisher@purdue.edu (T.S. Fisher).

0378-7753/$ – see front matter © 2012 Elsevier B.V. All rights reserved.
http://dx.doi.org/10.1016/j.jpowsour.2012.11.040

high material cost, which derives from the scarcity of Ru. Conversely, MnO_2, with low cost, low toxicity, and most importantly high theoretical specific capacitance ($\sim$1370 F g^{-1}) [7] has attracted much attention as a pseudocapacitive electrode material. However, its poor electric conductivity (10^{-5}–10^{-6} S cm^{-1}) and its tendency to function capacitively in thin surface layers create practical challenges to realizing its high theoretical capacitance [7]. Nonetheless, numerous studies aimed at realizing favorable new microstructures on MnO_2-based composites for use as electrodes have been reported on both flexible and rigid substrates [8–16].

Carbon materials (*e.g.*, carbon nanotubes [3,17], carbon fibers [18], activated carbon [19], graphene [20–22]) are widely studied as supercapacitor electrodes due to high specific area, high conductivity and low mass density. Among these, vertical graphene nanosheets or graphitic petals (GPs) directly grown on carbon cloth or Ni foil without any binder have shown promising results as active electrode materials in ECs [23–25]. However, to date, this highly conductive and two-dimensional (2-D) carbon nanosheet structure as a nanotemplate has not yet been systematically studied and optimized to exploit the electrochemical properties of the pseudocapacitive materials (*e.g.*, metal oxide).

In this paper, we report the EC performance of vertical GPs grown by microwave plasma chemical vapor deposition (MPCVD) on flexible commercial buckypaper (BP). The BP provides a light, flexible, and mechanically robust substrate for GP growth. This substrate, when coated with a thin MnO_2 layer, forms an architecture referred to as a MnO_2/GP/BP composite electrode. The GP/BP architecture offers an effective scaffold for exploiting the outstanding electrochemical behavior of MnO_2, realizing high energy and power density characteristics for electrochemical supercapacitor applications.

Density functional theory (DFT) calculations were carried out to provide further insight on the interfacial electrical nature of the MnO_2 on the surface of GPs. The DFT results show a MnO_2/graphene interface capable of electron transport during the charge/discharge process.

2. Experimental

The MPCVD system used for synthesis of GPs in this study has been previously described in detail elsewhere [26]. To our best knowledge, the formation of petals requires a plasma environment, and this need likely explains the limited prior work on GPs for electrochemical storage, as non-plasma CVD of planar graphene is a much more common and inexpensive laboratory method. Briefly, the plasma source consists of a 2.45 GHz frequency microwave power supply with variable power. Commercial buckypaper (Nanocomp Technologies, Inc., USA), washed in 6 M HNO_3 for 15 min to eliminate the residuals and surfactant before GP growth, was used as substrates to grow GPs. The substrates, elevated 9 mm above a Mo puck by ceramic spacers, were subjected to MPCVD conditions of H_2 (50 sccm) and CH_4 (10 sccm) as the primary feed gases at 30 Torr total pressure. The substrates were initially exposed to hydrogen plasma for approximately 2 min, during which the plasma power gradually increased from 300 W to 600 W. The GP growth duration was 20 min. The typical dimensions of the samples were 15 mm $\times$ 5 mm.

To make GP/BP composites suitable for electrochemical electrodes prior to MnO_2 coating or electrochemical measurement, concentrated H_2SO_4 and HNO_3 (volume ratio 3:1) were used to functionalize the surface of GPs at 50 °C for 2 h in an oven. The samples were then washed in deionized water and dried at 100 °C overnight. A neutral precursor solution (pH 7) for the MnO_2 coating process was prepared by mixing 0.1 M Na_2SO_4 (Alfa Aesar) and 0.1 M $KMnO_4$ (Alfa Aesar) solutions. The GPs grown on BP were immersed into the solution, which was kept at 80 °C in an oven for 40 min. The loading amount can be easily controlled by adjusting the immersion time. The sample was then rinsed with deionized water and subsequently annealed at 200 °C for 3 h using a hotplate in air. The mass of coated MnO_2 was calculated from the weight difference before and after the coating process. The loading amount of MnO_2 in this study is approximately 110 μg, measured using a microbalance with an accuracy of 1 μg.

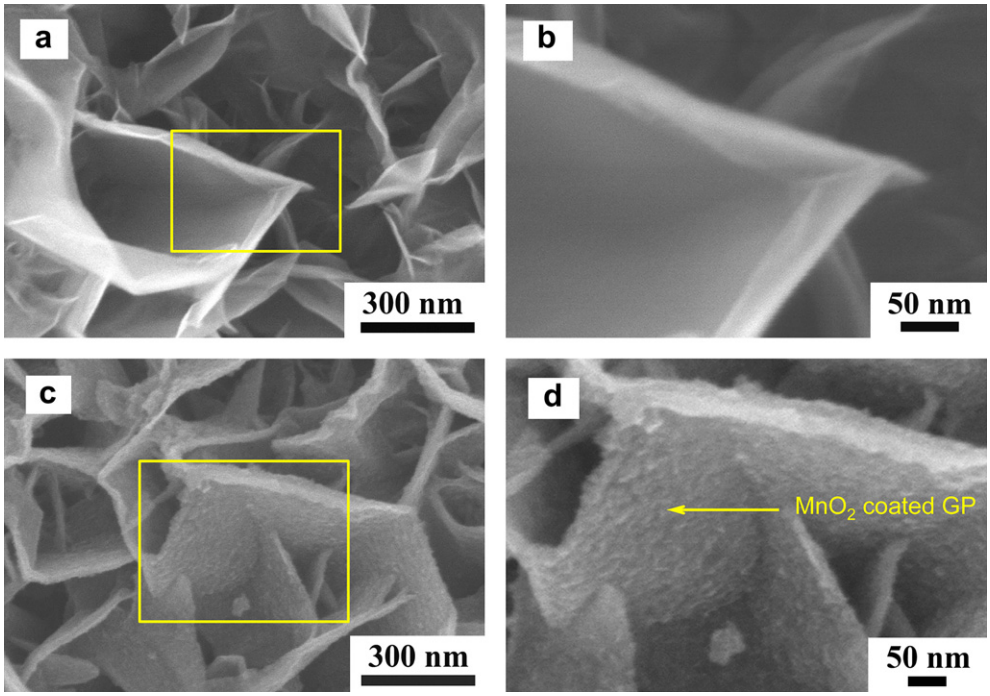

Fig. 1. SEM images of (a) graphitic petals. (b) A magnified image of graphitic petals showing smooth surfaces. (c) MnO_2 coated on graphitic petals. (d) A magnified image of uniform MnO_2 coating on graphitic petals.

The electrochemical performance of the MnO_2/GP/BP hybrid structure was evaluated using a BASi Epsilon electrochemical system (Bioanalytical Systems Inc., Indiana, USA). The standard three-electrode cell consisted of Ag/AgCl as the reference electrode, Pt mesh as the counter electrode and the synthesized composite sample as the working electrode. A 1 M Na_2SO_4 solution served as the electrolyte at room temperature. Scan rates of 2, 5, 10, 20, 50, and 100 mV s^{-1} were employed for cyclic voltammetry, and charge/discharge measurements were carried out at different current densities of 5, 10, 20, 30, 40 and 50 A g^{-1}. Long-term cyclic stability of the composite electrodes was evaluated repeatedly at 100 mV s^{-1} for 1000 cycles. A potential window in the range from 0 to 0.8 V was used in all measurements. A Hitachi S-4800 field emission scanning electron microscope (FESEM) was used to image the surface morphology of all the samples.

Throughout this study, multiple samples were prepared under identical conditions to test for reproducibility of the processing conditions. CV data acquired from the multiple samples could be reproduced to within ±5%. In what follows, we present the best results chosen from the sample set.

3. Modeling

To understand the electronic structure of the MnO_2/GP composite, we have simulated large clusters of (4 × 2) MnO_2 on a graphene supercell (6 × 6) using density function theory (DFT). Although in real cases the MnO_2 structure displays diverse conformations with edge-and corner-sharing MnO_6 possessing various pore sizes [27–31], with a distribution of Mn cations among the network of oxygen atoms, we employed the simplest

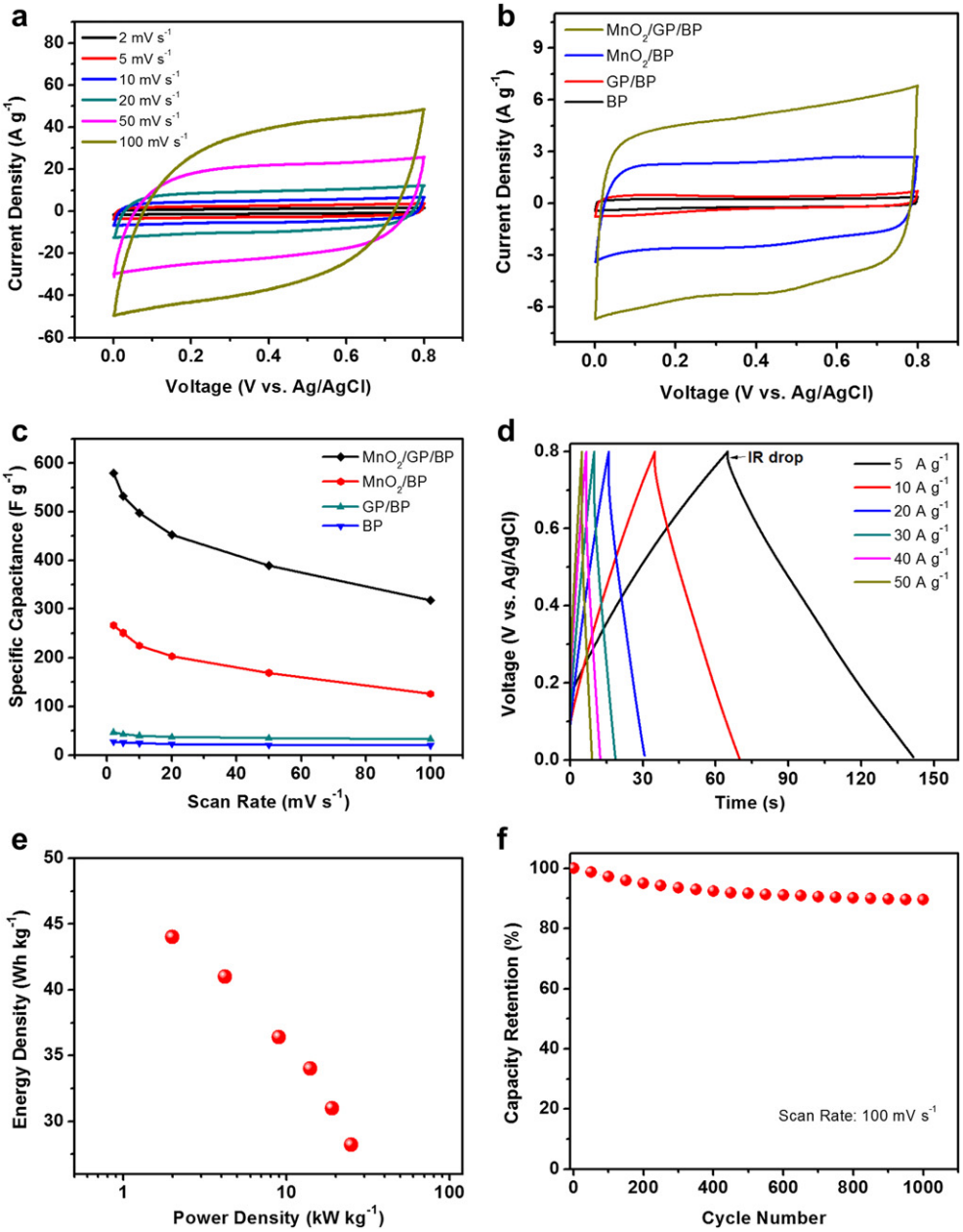

Fig. 2. (a) Cyclic voltammetry curves of the MnO_2/GP/BP composites at different scan rates in 1 M Na_2SO_4 aqueous electrolyte. (b) Cyclic voltammetry curves of BP, GP/BP, MnO_2/BP, and MnO_2/GP/BP at 10 mV s^{-1}. (c) Specific capacitances of MnO_2/GP/BP (black), MnO_2/BP (red), GP/BP (dark cyan) and BP (blue) at different scan rates. (d) Charge/discharge curve of MnO_2/GP/BP at different current densities. (e) Ragone plot of the estimated specific energy and specific power at various current densities. (f) Capacity retention of MnO_2/GP/BP as a function of cycle number. (For interpretation of the references to color in this figure legend, the reader is referred to the web version of this article.)

configuration. Electronic structure calculations were carried out by DFT with the plane-wave self-consistent field (PWSCF) code [32]. The generalized gradient approximation (GGA) [33] was implemented to estimate the exchange correlation energy of electrons. Ultrasoft pseudopotentials [34] were used to represent the interaction between ionic cores and valence electrons. Kohn-Sham wave functions were represented with a plane-wave basis using an energy cutoff of 40 Ry and charge density cutoff of 240 Ry [35]. A uniform mesh of k points ($5 \times 5 \times 1$) was taken for integration over the Brillouin zone [36].

4. Results and discussion

SEM images of GPs synthesized by MPCVD are shown in Fig. 1a. The petals extend approximately 500 nm from the BP surface, and the typical span width of a single unwrinkled 2-D petal ranges from 100 nm to 500 nm. The thickness of a GP can reach several nanometers, corresponding to less than 50 graphene layers. A magnified image of one petal marked by the rectangular box in Fig. 1a is shown in Fig. 1b, revealing the smooth surfaces of the GPs. These surfaces provide easily accessible sites for MnO_2 coating. The crumpled structures of the vertical graphene sheets with both sides exposed to MnO_2 precursor solution offer large specific area for coating. Fig. 1c shows the morphology of MnO_2 coated on GPs. Fig. 1d contains a magnified image of the area marked by the rectangular box in Fig. 1c, clearly showing a thin uniform layer of MnO_2 on the smooth GP surfaces, even on the smaller petals.

Previous studies [13,37] suggest that MnO_4^- ions can be reduced spontaneously to MnO_2 on the surface of carbon nanotubes by oxidizing exterior carbon atoms via the following redox reaction:

$$4MnO_4^- + 3C + H_2O \leftrightarrow 4MnO_2 + CO_3^{2-} + 2HCO_3^- \quad (1)$$

We believe that a similar mechanism applies here in the case of MnO_2 coating on GP surfaces. Reduction of permanganate ion (MnO_4^-) to MnO_2 on carbon is pH-dependent. Neutral pH solution leads to thin films of MnO_2, while acidic solution can result in large agglomerated MnO_2 particles [13]. Consequently, the thin film of MnO_2 coated on GPs can be attributed to the neutral electrolyte used in this study.

Fig. 2a shows cyclic voltammetry (CV) curves of the MnO_2/GP/BP composites at scan rates of 2, 5, 10, 20, 50, 100 mV s^{-1} in 1 M Na_2SO_4 aqueous solution with potential windows ranging from 0 to 0.8 V. The advantages of the unique electrochemical behaviors of MnO_2/GP/BP electrodes are apparent in Fig. 2b which shows a comparison of CV curves for BP, GP/BP, MnO_2/BP and MnO_2/GP/BP at a fixed scan rate of 10 mV s^{-1}. The shapes of these curves are quasi-rectangular, indicating the presence of electrical double-layer capacitance and pseudocapacitance. The MnO_2-coated GP/BP architecture involves redox reactions in the cyclic voltammetry tests as Mn atoms are converted into higher/lower (IV/III) oxidation states. These conversions are induced by intercalation/extraction of H_3O^+ or alkali cations (Na^+) to/from the MnO_2 outer layer. The mechanism of this reaction can be expressed as [7,11,38]:

$$(MnO_2)_{surface} + X^+ + e^- \leftrightarrow (MnOOX)_{surface} \quad (X^+ = Na^+ \text{ or } H_3O^+) \quad (2)$$

The average specific capacitance from CV curves was determined by [9]:

$$C = \frac{1}{2sM(V_h - V_l)} \oint_{V_l \to V_h \to V_l} I(V)\mathrm{d}V \quad (3)$$

where C is the specific capacitance in F g^{-1}, s is the scan rate in V s^{-1}, M is the mass of the added MnO_2 to the electrodes in g, V_h and V_l are high and low potential limits of the CV tests in V, I is the instantaneous current on CV curves, and V is the applied voltage (V). The specific capacitance of BP at a scan rate of 2 mV s^{-1} calculated from the CV curves is 27 F g^{-1}, which is comparable to reported values for CNTs [39]. The specific capacitance of GP/BP (based on total mass of the two components) calculated at 2 mV s^{-1} is 47 F g^{-1}, which is approximately 70% higher than that of bare BP. The same improvement (~70%) was also observed in H_2SO_4 electrolyte (results not shown here), indicating an inherent improvement in specific capacitance after GP growth on BP. This result is attributed to an increase in the specific area after growing GPs on the BP substrate coupled with electric field enhancement introduced by the sharp edges of the GPs.

The specific capacitance of the MnO_2/GP/BP composites was calculated based on the mass of pristine MnO_2 for the following reasons: (1) The surface of carbon was coated with MnO_2; consequently, the carbon materials would participate weakly in the charge storing process as charge is primarily stored at the outer layer of MnO_2 through a Faradic reaction. (2) The specific capacitances of BP and GP/BP are mainly of the electrostatic double-layer type and are far smaller than the specific capacitance of MnO_2 caused by Faradic redox reactions, making it reasonable to calculate the specific capacitance based on the mass of pristine MnO_2.

Fig. 2c shows comparative specific capacitances of BP, GP/BP, MnO_2/BP and MnO_2/GP/BP calculated from CV curves at voltage scan rates from 2 to 100 mV s^{-1}. At a scan rate of 2 mV s^{-1}, the specific capacitance of the MnO_2/GP/BP hybrid composite reaches 580 F g^{-1} (based on the mass of pristine MnO_2). The specific capacitance based on the overall mass (MnO_2/GP/BP) at 2 mV s^{-1} is 218 F g^{-1}, which is higher than that of a comparable MnO_2/BP composite previously reported [16]. The masses of the composite constituents through the integration process for a typical sample are provided in Table 1. At a high scan rate of 100 mV s^{-1}, the specific capacitance of MnO_2/GP/BP still remains close to 320 F g^{-1}, which is comparable to the rate performance reported elsewhere [8,9,11,14]. However, for the same MnO_2 coating time, the specific capacitance of MnO_2/BP is only about 266 F g^{-1} (based on pristine MnO_2) at 2 mV s^{-1} (see Fig. 2c). The superior rate capability of MnO_2/GP/BP composites demonstrates the advantages of this new architecture of GP/BP as a highly conductive scaffold for maximizing the utilization of the practical electrochemical performance of MnO_2. Since previous studies show that only a very thin layer of MnO_2 is involved in the charge storage process [7], the specific capacitance of MnO_2 coated on the supporting GP/BP can likely be further improved by optimizing the thickness of the coated MnO_2 layer.

Constant-current charge/discharge curves of the as-prepared MnO_2/GP/BP hybrid structure at different current densities are shown in Fig. 2d. The charge/discharge curves display a symmetric shape, indicating that the structure has a good electrochemical capacitive characteristic. The specific capacitance derived from galvanostatic (GV) tests can be calculated from [8]:

$$C = \frac{I_d}{M\upsilon} \quad (4)$$

where I_d is the discharge current in A, and υ is the slope of the discharge curve after the initial potential drop associated with the

Table 1
Area-normalized composite constituent masses for a typical sample with Euclidean area of 75 mm^2 measured by a microbalance with 1 μg accuracy.

	BP	GP + BP	MnO_2 + GP + BP
Mass (μg mm^{-2})	5.08	6.56	10.2

cell internal resistance (IR drop). The specific capacitances derived from the discharge curves agree well with the results calculated from CV measurements. At 5 A g^{-1}, the calculated specific capacitance is 493 F g^{-1}, which is almost identical to the specific capacitance 497 F g^{-1} calculated at 10 mV s^{-1}, corresponding to an average current density close to 5 A g^{-1} (see Fig. 2b).

The energy density E (in Wh kg^{-1}) and the power density P (in kW kg^{-1}) are important parameters to characterize the electrochemical performance of supercapacitors. In this study, these quantities were calculated by:

$$E = \frac{CV^2}{2M} \tag{5}$$

$$P = \frac{E}{\Delta t} \tag{6}$$

where V is the applied voltage in volts and Δt is the discharge time in seconds. Fig. 2e shows the Ragone plot for the MnO_2/GP/BP structured electrode at different current densities. At a high current density of 50 A g^{-1}, the calculated energy density is 28 Wh kg^{-1}, and the average power density is 25 kW kg^{-1}. These values are more promising than the reported energy density (14.8 Wh kg^{-1}) and power density (2.5 kW kg^{-1}) of electrodeposited MnO_2 films on BP substrates [14], suggesting that the MnO_2/GP/BP composite warrants further consideration as an electrode material in supercapacitor applications.

Cycle lifetime is one of the most critical factors in supercapacitor applications. Typical issues facing MnO_2-based electrodes in aqueous electrolyte include: mechanical expansion of MnO_2 during ion insertion/desertion processes, MnO_2 film detachment from electrode surfaces, and Mn dissolution into electrolyte [7,38]. A cyclic stability test over 1000 cycles for the MnO_2/GP/BP structured electrode at a scan rate of 100 mV s^{-1} was carried out in a potential window ranging from 0 to 0.8 V. Fig. 2f shows the specific capacitance retention as a function of cycle number. The composite electrode shows less than 10% loss in specific capacitance after 1000 charge/discharge cycles, indicating good capacity retention.

DFT simulations can help to elucidate the fundamental properties at interfaces between MnO_2 and graphene, particularly in terms of lattice stability and electronic structure of the composite. A schematic diagram of MnO_2 clusters and graphene (top view) is shown in Fig. 3a. In this configuration, constrained relaxation was carried out (only atomic positions of the MnO_2 are allowed to relax, with initially relaxed graphene). In order to focus on the interface between MnO_2 and graphene, we have considered only one layer of graphene and a simple MnO_2 cluster as shown in Fig. 3a, with the purpose of elucidating basic mechanisms that are possible at interfaces between MnO_2 and graphene. The MnO_2/GP composite is relaxed with energy converged to less than 2 kcal mol^{-1}. The formation energy of the composite is calculated to be 128 kcal mol^{-1}, suggesting covalent bonding between MnO_2 and graphene. During the charge/discharge process, we expect the composite to undergo compressive/tensile stresses. To mimic the phenomena, we have simulated the structure with various pressure values in the supercell. From the electronic density of states, the composite exhibits metallic behavior (finite density of states at E_F) in both cases, and this metallic state changes little with different stresses as shown in Fig. 3b, where different negative/positive pressures are used to mimic compressive/tensile stresses. We note that the present case of a thin MnO_2 layer on graphene is quite different from bulk MnO_2 and a graphitic interface, for which further complexities arise. The comparative electronic density of states of graphene, MnO_2 and MnO_2/graphene (the most stable structure) are shown in Fig. 3c.

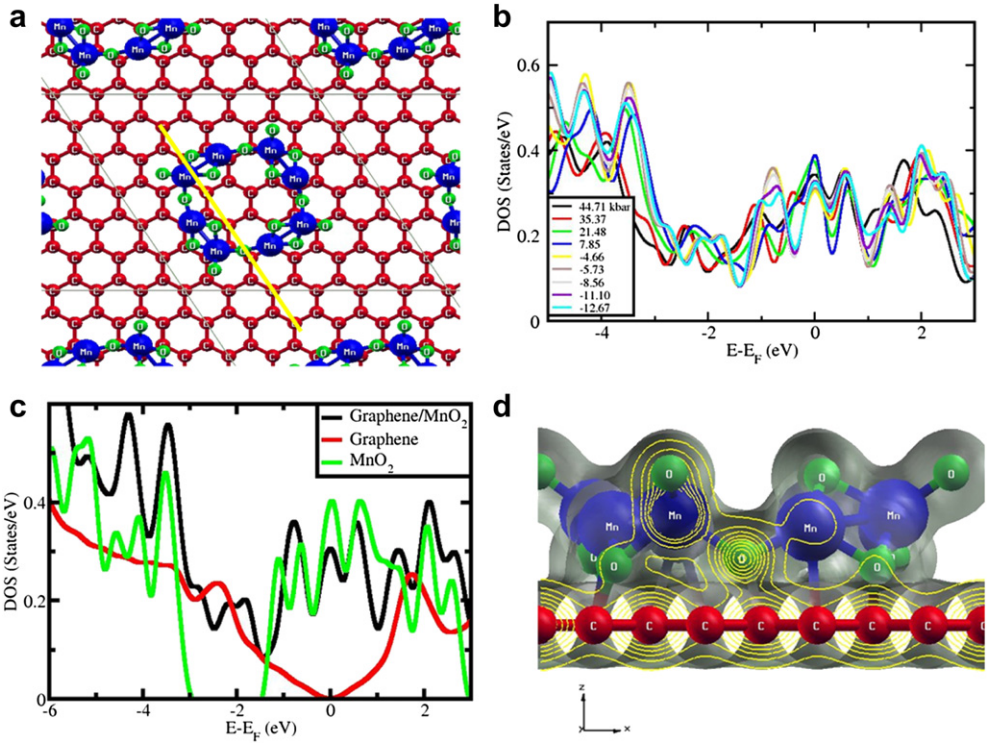

Fig. 3. (a) Schematic diagram of MnO_2 clusters and graphene (top view); (b) Electronic density of states under compressive/tensile stresses (c) the comparative electronic density of states of graphene, MnO_2 and MnO_2/graphene; (d) Iso-electronic charge contour plot shown at a particular plane (indicated by the yellow line from the top view in (a), perpendicular to the graphene plane and along a zig-zag direction) with electronic charge distribution at MnO_2/graphene interface. (For interpretation of the references to color in this figure legend, the reader is referred to the web version of this article.)

The low interfacial resistance achieved in the MnO_2/GP/BP electrode is a matter of interest, and we use the results of DFT calculations to provide further insight into this result. The iso-electronic charge contour plot drawn in Fig. 3d is a two-dimensional cut of the charge density in a vertical plane that contains the yellow line drawn parallel to the zig-zag direction as shown in Fig. 3a. This vertical plane was chosen to highlight the redistribution of charge from the graphene layer toward the oxygen atoms in MnO_2. Further iso-electronic contour plots in different planes are provided in the Supplementary information. From these plots, we infer that charge transfer at the graphene-MnO_2 interface is facilitated by the oxygen atoms in the MnO_2 complex, providing some understanding for the low interfacial resistance experienced by electron transport through the composite interface. Without this conduction channel, charge transfer would be reduced, making the composite less suitable for supercapacitor applications.

5. Conclusion

A new structure of MnO_2/GP/BP has been demonstrated for flexible supercapacitor electrodes, showing promising electrochemical behavior. The GP/BP architecture without any binder provides an efficient scaffold for maximizing the practical electrochemical performance of MnO_2, realizing high specific capacitance, excellent rate capability and long-term cycle life, high energy density and high power density. The metallic nature of the MnO_2/GP composite provides a facile conduction path for electron transport in the charge/discharge process. These results suggest that such a MnO_2/GP/BP architecture may be practically useful for next generation high-performance supercapacitors.

Acknowledgments

The authors thank the U.S. Air Force Research Laboratory (AFRL), and its Office of Scientific Research (AFOSR) under the MURI program on Nanofabrication of Tunable 3D Nanotube Architectures (PM: Dr. Joycelyn Harrison), for financial support in this work. The authors also thank Dr. Chuizhou Meng and Ritu Gupta for the useful discussions. We acknowledge use of the xcrysden computer graphic tool for visualizing the structures (www.xcrysden.org) [40].

Appendix A. Supplementary data

Supplementary data related to this article can be found at http://dx.doi.org/10.1016/j.jpowsour.2012.11.040.

References

[1] P. Simon, Y. Gogotsi, Nat. Mater. 7 (2008) 845–854.
[2] B.E. Conway, Electrochemical Supercapacitors: Scientific Fundamentals and Technological Applications, Kluwer Academic/Plenum Publishers, New York, 1999.
[3] J. Li, N. Wang, Y. Zhao, Y. Ding, L. Guan, Electrochem. Commun. 13 (2011) 698–700.
[4] J.P. Zheng, P.J. Cygan, T.R. Jow, J. Electrochem. Soc. 142 (1995) 2699–2703.
[5] J.M. Li, K.H. Chang, C.C. Hu, Electrochem. Commun. 12 (2010) 1800–1803.
[6] K. Xie, J. Li, Y. Lai, W. Lu, Z. Zhang, Y. Liu, L. Zhou, H. Huang, Electrochem. Commun. 13 (2011) 657–660.
[7] M. Toupin, T. Brousse, D. Belanger, Chem. Mater. 16 (2004) 3184–3190.
[8] G. Yu, L. Hu, M. Vosgueritchian, H. Wang, X. Xie, J.R. McDonough, X. Cui, Y. Cui, Z. Bao, Nano Lett. 11 (2011) 2905–2911.
[9] L. Bao, J. Zang, X. Li, Nano Lett. 11 (2011) 1215–1220.
[10] X. Lang, A. Hirata, T. Fujita, M. Chen, Nat. Nanotechnol. 6 (2011) 232–236.
[11] J. Yan, E. Khoo, A. Sumboja, P.S. Lee, ACS Nano 4 (2010) 4247–4255.
[12] Y. Hou, Y. Cheng, T. Hobson, J. Liu, Nano Lett. 10 (2010) 2727–2733.
[13] S.W. Lee, J. Kim, S. Chen, P.T. Hammond, Y.S. Horn, ACS Nano 4 (2010) 3889–3896.
[14] K.W. Nam, C.W. Lee, X.Q. Yang, B.W. Cho, W.S. Yoon, K.B. Kim, J. Power Sources 188 (2009) 323–331.
[15] H. Zhang, G. Cao, Z. Wang, Y. Yang, Z. Shi, Z. Gu, Nano Lett. 8 (2008) 2664–2668.
[16] S.L. Chou, J.Z. Wang, S.Y. Chew, H.K. Liu, S.X. Dou, Electrochem. Commun. 10 (2008) 1724–1727.
[17] C. Meng, C. Liu, S. Fan, Electrochem. Commun. 11 (2009) 186–189.
[18] Y. Chen, Y. Hsu, Y. Lin, Y. Lin, Y. Horng, L. Chen, K. Chen, Electrochim. Acta 56 (2011) 7124–7130.
[19] A. Yuan, Q. Zhang, Electrochem. Comm. 8 (2006) 1173–1178.
[20] L.T. Le, M.H. Ervin, H. Qiu, B.E. Fuchs, W.Y. Lee, Electrochem. Commun. 13 (2011) 355–358.
[21] C. Liu, Z. Yu, D. Neff, A. Zhamu, B.Z. Jang, Nano Lett. 10 (2010) 4863–4868.
[22] J.J. Yoo, K. Balakrishnan, J. Huang, V. Meunier, B.G. Sumpter, A. Srivastava, M. Conway, A.L.M. Reddy, J. Yu, R. Vajtai, P.M. Ajayan, Nano Lett. 11 (2011) 1423–1427.
[23] J.R. Miller, R.A. Outlaw, B.C. Holloway, Science 329 (2010) 1637–1639.
[24] X. Zhao, H. Tian, M. Zhu, K. Tian, J.J. Wang, F. Kang, R.A. Outlaw, J. Power Sources 194 (2009) 1208–1212.
[25] T.C. Hung, C.F. Chen, W.T. Whang, Electrochem. Solid State Lett. 12 (2009) K41–44.
[26] G. Xiong, K.P.S.S. Hembram, D.N. Zakharov, R.G. Reifenberger, T.S. Fisher, Diam. Relat. Mater. 27–28 (2012) 1–9.
[27] S. Devaraj, N. Munichandraiah, J. Phys. Chem. C 112 (2008) 4406–4417.
[28] H.Y. Lee, J.B. Goodenough, J. Solid State Chem. 144 (1999) 220–223.
[29] F. Cheng, J. Zhao, W. Song, C. Li, H. Ma, J. Chen, P. Shen, Inorg. Chem. 45 (2006) 2038–2044.
[30] X. Wang, Y. Li, Chem. Eur. J. 9 (2003) 300–306.
[31] J.C. Hunter, J. Solid State Chem. 39 (1981) 142–147.
[32] S. Baroni, A. Dal Corso, S. de Gironcoli, P. Gianozzi, http://www.pwscf.org.
[33] J.P. Perdew, K. Burke, M. Ernzerhof, Phys. Rev. Lett. 77 (1996) 3865–3868.
[34] D. Vanderbilt, Phys. Rev. B 41 (1990) 7892–7895.
[35] M. Methfessel, A. Paxton, Phys. Rev. B 40 (1989) 3616–3621.
[36] H.J. Monkhorst, J.D. Pack, Phys. Rev. B 13 (1976) 5188–5192.
[37] X. Jin, W. Zhou, S. Zhang, G.Z. Chen, Small 3 (2007) 1513–1517.
[38] A. Era, Z. Takehara, S. Yoshizawa, Electrochim. Acta 12 (1967) 1199–1212.
[39] R. Shah, X. Zhang, S. Talapatra, Nanotechnology 20 (2009) 395202. art.no.
[40] A. Kokalj, Comp. Mater. Sci. 28 (2003) 155–168.